

Promising Perspectives on the Use of Fullerenes as Efficient Containers for Beryllium Atoms

Igor Bodrenko, Alessandra Satta,* Claudia Caddeo, Giacomo Cozzolino, Stefan Milenkovic, Matteo Ceccarelli, and Alessandro Mattoni*

The possibility of using fullerenes as containers for toxic beryllium atoms is studied by a multi-scale approach in which first-principles and classical molecular dynamics simulations are combined. By studying the energetics, electronic and spectroscopic properties of Be-fullerene systems and by simulating their interaction at finite temperature in vacuo and in representative biological environments it is concluded that: i) Be endohedral complexes can be obtained by implanting Be atoms at energies >2.3 eV that is consistent with laser implantation technologies; ii) it is in principle possible to distinguish stable endohedral complexes from metastable exohedral ones by optical absorption, suggesting that optical spectroscopy can be a valuable non-destructive technique to assist the synthesis and the control of implanted films iii) the Be-endohedral complexes are long-lived and thermodynamically stable and can confine beryllium both in vacuo and in aqueous solution; iv) Be@C60 complexes are likely unable to penetrate the selectivity filters of a prototypical protein showing that fullerene prevents undesired interactions with biomolecules and toxicity effects of Be²⁺ related to replacement of the Ca²⁺. Overall, these results provide an assessment on the possibility to encapsulate Be atoms into fullerenes by ion implantation to synthesize inert and highly stable and safe molecular containers for toxic beryllium radionuclides. Great opportunities are expected for the realization and application of Be-C60 complexes to nanotechnology and nanomedicine with particularly appealing perspectives in the field of neutron capture therapy of cancer.

1. Introduction


Carbon fullerenes can encapsulate a wide variety of atoms, ions, clusters, or small molecules, resulting in stable compounds with novel structures and electronic properties, which are referred to as endohedral fullerenes.^[1] The first endohedral C60 complex, called La@C60, featured a lanthanum atom and it was synthesized in 1985.^[2] Early works on endohedral fullerenes focused on encapsulating metals inside the carbon cages through laser vaporization of graphite/metal structures or via arc discharge methods.^[3] Incorporation of noble gasses in C60 and C70 was also considered and achieved by means of high pressure.^[4] Few years later it was reported the implantation of ⁷Be into C60.^[5] Endohedral fullerenes have been proposed for applications which range from quantum computing^[6,7] to magnetic resonance imaging contrast agents,^[8] to use in selective irradiation of tumors through neutron capture.^[9,10] Beryllium-doped endohedral fullerenes ⁷Be@C60 have been suggested for application in neutron capture therapy (NCT)^[11] as substitutes of boron isotope ¹⁰B.^[12,13,14,15] Boron NCT technology is limited due to the difficulty to identify

B-containing compounds that can be accumulated in the tumor cells, and to the fact that BNCT requires high enough neutron flux (10^{10} to 10^{12} cm⁻² s⁻¹) not well suited for systematic massive clinical studies.^[14–18] The neutron absorption cross section for ⁷Be is more than 10 times higher than for ¹⁰B.^[19,20] This would allow it to deposit a smaller number of ⁷Be nuclides per cell, at the same neutron flux and exposition time, or to reduce the intensity of neutron flux while keeping the nuclide concentration in the tumor the same as for ¹⁰B. The drawback of using Be is its toxicity. At physiological conditions the Be atoms get oxidized into Be²⁺ easily interacting with many tissues and cells, where it specifically targets cell nuclei, inhibiting many enzymes, including those used for synthesizing DNA.^[21] The possibility to use Be atoms requires strategies to prevent its chemical interaction with the tissues and cells.

Here we study the Be encapsulation into C60 as an efficient strategy to hinder its unwilling interaction with biomolecules. We focus on the case of neutral Be atoms as a first study. We explore

I. Bodrenko, A. Satta, C. Caddeo, G. Cozzolino, S. Milenkovic, M. Ceccarelli, A. Mattoni
Cnr-Istituto Officina dei Materiali
Unità di Cagliari (CNR-IOM)
Cittadella Universitaria
Monserrato I-09042, CA, Italy
E-mail: alessandra.satta@cnr.it; mattoni@iom.cnr.it

G. Cozzolino, S. Milenkovic, M. Ceccarelli
Dipartimento di Fisica
Università di Cagliari
Cittadella Universitaria
Monserrato I-09042, CA, Italy

 The ORCID identification number(s) for the author(s) of this article can be found under <https://doi.org/10.1002/adfm.202303786>

© 2023 The Authors. Advanced Functional Materials published by Wiley-VCH GmbH. This is an open access article under the terms of the Creative Commons Attribution License, which permits use, distribution and reproduction in any medium, provided the original work is properly cited.

DOI: 10.1002/adfm.202303786

the possibility to realize ${}^7\text{Be}@C60$ endohedral fullerenes and provide estimates on insertion energy and on the stability of such complexes. On the one hand, it is important to characterize the energy necessary to form the complexes in order to determine efficient synthesis strategies; on the other hand, it is necessary to estimate the lifetime of such complexes to avoid unwanted Be outcome from fullerenes whether they contain defects or not. It is also important to exclude the formation of metastable complexes in which beryllium is bound to fullerenes but not confined.

The formation of ${}^7\text{Be}@C60$ complexes via a nuclear recoil reaction has been reported in literature.^[5] Ab initio molecular dynamics was used to model the insertion of a ${}^7\text{Be}^{2+}$ ion with 5 eV kinetic energy. Other studies investigated the structural and electronic ground state of Be in $C60$ ^[22,23] or other bigger fullerene-like cages with slightly different results on the minimum energy position.^[24,25,26] In the perspective of Be confinement there is a lack of knowledge, especially on the exact energy barriers necessary to insert/extract Be into the fullerenes, the lifetime of such complexes, and their optical properties.

In this work, we provide a robust theoretical assessment of the possibility of using fullerenes as containers for beryllium. To this aim we adopt a multi-scale approach in which we combine first-principles and classical molecular dynamics simulations at finite-temperature. We perform a comprehensive characterization in terms of energetics, electronic and spectroscopic properties by means of state-of-the-art Density Functional Theory (DFT) simulations, and we develop a classical force field that reproduces the Be-C interactions and energy barriers for insertion which allows us to simulate the Be implantation process at room temperature and to estimate the lifetime of the ${}^7\text{Be}@C60$ complexes. We show that Be endohedral fullerenes can be obtained by implanting Be atoms at energies >2.3 eV, and the so-formed complexes are long-lived and thermodynamically stable, with lifetimes exceeding average human life expectancy. Furthermore, our calculations show that it is possible to distinguish endohedral, exohedral and unbound Be-C60 pairs by optical absorption, suggesting non-destructive optical spectroscopy as a valuable tool for the control of implanted films. Overall, our results on Be-C60 represent a first step toward a more general study of Be-fullerene interaction but already provide an assessment on the possibility to efficiently encapsulate Be atoms into fullerenes to synthesize highly stable molecular containers for beryllium radionuclides.

2. Structure and Energetics of C60/Be Endohedral and Exohedral Complexes

As a first step, we identify and characterize the lowest energy configurations of Be inside and outside C60. To this aim we performed a comprehensive characterization of Be/C60 stationary configurations at various levels of ab initio theory by manually seeding initial configurations of Be followed by geometry optimization, see Supporting Information (SI). The harmonic vibrational frequencies in the local minima were calculated to differentiate local minima and saddle points. We used Gaussian16 software package to perform these calculations.^[27] The Restricted Hartree Fock (RHF) method was considered, as well as four exchange and correlation functionals including standard LDA and PBE^[28] and PBE-D3BJ^[29] and the hybrid functional B3LYP.^[30]

PBE-D3BJ accounts for the empirical Van der Waals interaction correction, which is important for comparing the relative energies of the configurations. The 6–31G* Gaussian basis set^[31] was used and the PBE-D3BJ functional was eventually chosen as the reference method for studying energetics, representing a good compromise between cost and accuracy. Among the stationary configurations studied with Be inside and outside the fullerene molecule, we selected those with the lowest energy: two distinct stationary geometries of Be-endofullerene, one with Be in the center (denoted as “ ${}^7\text{Be}@C60$ in-1” in **Figure 1a**) and the second off center (denoted as “ ${}^7\text{Be}@C60$ in-2”).

The ${}^7\text{Be}@C60$ in-1 structure has the lowest energy of -0.67 eV with respect to the separated Be and C60 (PBE-D3BJ). The large Be-C60 distance (3.56 Å) and the unaffected electronic charge, Δq_{Be} , on the Be atom (see **Table 1**) suggest that there is no orbital mixing between Be and C60 in this configuration. This is consistent with previous findings,^[22,32] where the Be occupying the center of the fullerene turns out to be the most stable configuration. In the second lowest-energy endohedral structure (${}^7\text{Be}@C60$ in-2, **Figure 1b**), the Be atom is slightly off-center, at ≈ 1.7 Å from to the nearest carbon. The energy of this configuration is 0.31 eV higher than that of ${}^7\text{Be}@C60$ in-1. The equivalent geometry, found by Morisato et al.^[32] via linear combination of the atomic orbital LCAO method, reflects the same trend in terms of stability of configurations but results in a significantly smaller energy difference (0.01 eV) between ${}^7\text{Be}@C60$ in-2 and ${}^7\text{Be}@C60$ in-1. Such a discrepancy is likely to be attributed to the different basis sets involved in the adopted methods. Moreover, in structure ${}^7\text{Be}@C60$ in-2 there is a relevant Mulliken charge (+0.39) on Be that suggests orbital mixing between Be and C60. Finally, among the exohedral ones we have identified one stable configuration, the structure ${}^7\text{Be}@C60$ out-1, which is the most strongly bound exohedral complex with a binding energy of -0.22 eV.

Another configuration (${}^7\text{Be}@C60$ out-2), that is energetically unfavorable by ≈ 0.2 eV with respect to dissociation into separated Be – C60 moieties is reported in the Supporting Information.

The ${}^7\text{Be}@C60$ out-1 consists of Be atoms placed on top of a C–C dimer between one hexagon and one pentagon with the formation of two Be-C links. The binding involves electronic coupling of Be and C orbitals (see below) but due to the electronic stability of C60 the energy gain is relatively low (ca 0.3 eV) with a sizeable contribution from dispersive interactions. Such a relatively low binding energy is however sufficient to keep the exohedral complex stable at room temperature (energy barrier >0.3 eV, see below). From the applicative point of view in the context of NCT, such configuration is undesired as it can be dissociated by releasing toxic Be into the human body. It is necessary to post-process C60/Be films to discard these complexes.

Such configurations can be, in principle, discriminated by different spectroscopic techniques. In particular, electron spectroscopy technique (i.e., XPS, EELS) can discriminate configurations by the first ionization energies. In this regard, the calculated HOMO energy values (see **Table 1**) that give the estimate of the first ionization energies, suggest that the difference, being in the order of magnitude of 1–2 eV, could be experimentally resolved. Also, the optical absorption spectrum potentially can be used to distinguish among different configurations, as we will show in the following.

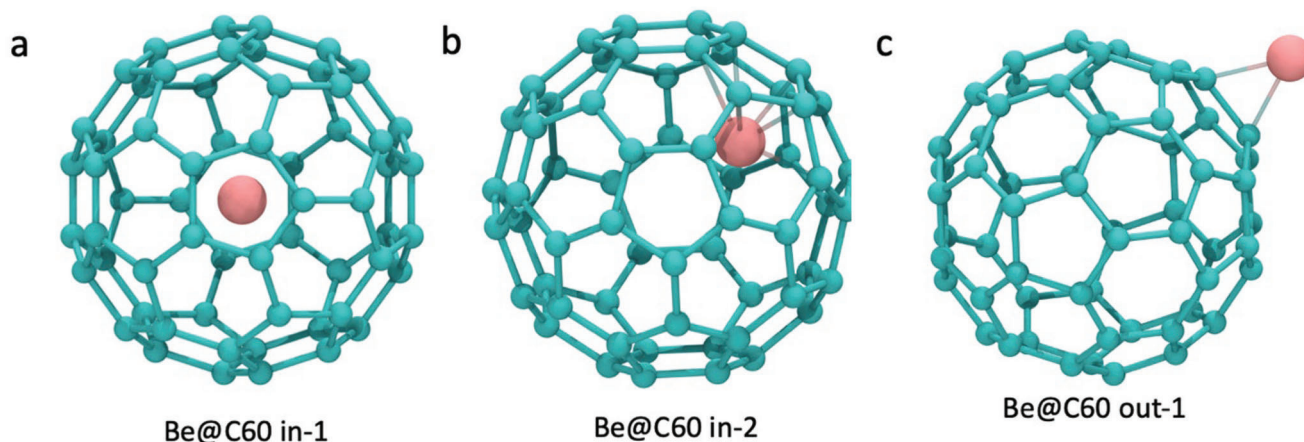


Figure 1. 3D view of the structures of the stationary points of endohedral Be@C60 a,b) and exohedral c) Be@C60 complexes.

3. Optical Properties

Optical spectroscopy is a non-destructive technique which can be used to differentiate between possible structures,^[33] provided that a reference is available. Theoretical calculation of the optical absorption spectra allows a direct comparison with experiments. The optical properties of the complex system C60/Be with Be atom in different positions with respect to the C60 molecule, the isolated C60 molecule and Be atom, respectively, have been investigated from first principles via time-dependent density functional theory (TDDFT) as implemented in quantum-ESPRESSO (QE) suite of open-source computer codes.^[34,35] The computational setup includes a cubic box of 21.2 Å containing the Be@C60 structures illustrated in Figure 1, including the isolated Be and C60 calculated separately. Convergence tests with increasing size of the box were made in order to avoid any interaction between images due to the periodic boundary conditions. The Kohn-Sham equations were solved by using a plane-waves basis set within the framework of a standard DFT-PBE computation with the use of norm-conserving pseudopotentials. A kinetic energy cutoff for the electron wavefunctions as large as 80 Ry was enough to ensure the total energy convergence. The Brillouin zone sampling was performed with a Monkhorst-Pack sampling with a mesh of $1 \times 1 \times 1$ (Γ point). Spin polarization of the electronic orbitals was included in the calculations. To obtain

Table 1. Characteristics of stationary geometries of Be@C60 in the endohedral (structures labeled as “in-1” and “in-2” in Figure 1) and exohedral (“out-1” in Figure 1) forms. ΔE is the electronic energy with respect to the isolated Be and C60; Δq_{Be} is the Mulliken charge on the Be atom due to the interaction with C60 (negative values of Δq_{Be} are increments of the electronic density); d is the distance between the Be atom and the nearest C atom; HOMO (highest occupied molecular orbital) energies obtained via RHF.

	Be@C60 in-1	Be@C60 in-2	Be@C60 out-1
ΔE (eV)	−0.67	−0.36	−0.22
Δq_{Be} (e^-)	−0.05	0.39	0.11
d (Å)	3.56	1.73	1.61
HOMO (eV)	−7.66	−5.77	−6.57

the optical spectrum for each mentioned structure, the Liouville-Lanczos approach was used since it has the advantage of giving direct access to the observable spectrum avoiding the explicit computation of the ground state unoccupied states. The absorption spectra are calculated as $I(\omega) \propto \omega \text{Im}(\alpha(\omega))$, where $\alpha(\omega)$ is the spherical average of the dipole polarizability. For the optical absorbance spectrum in the linear response regime, 20 000 Lanczos steps were used to obtain converged spectra. Results are shown in Figure 2, where the computed absorption coefficient for the isolated Be atom (top panel, a) and the isolated C60 molecule (panel b) are reported with respect to the wavelength of the incident photon, along with those obtained from the complexes Be@C60 with endohedral Be (in-1 and in-2, Figure 2c,d), and exohedral Be (out-1, Figure 2e), respectively.

The capital letters in Figure 2 (G, F, E, C), refer to the main features in the optical absorption spectra of C60 (see reference^[36]) whose major absorbance computed bands are reported in Table 2 along with those obtained for all the Be@C60 complexes. The vertical cyan and red lines indicate the positions of the isolated C60 and Be absorbance peaks throughout the spectra in Figure 2 and will be taken as references. Isolated Be (Figure 2a) shows a main absorption peak centered at 253 nm that can be ascribed to the allowed transition $2s2-2s2p$ in good agreement with the experimental estimate of 235 nm (see Table 8 in references^[37,38]). The present results for the isolated C60 compare excellently to those obtained with a similar method^[39] and show a reasonable agreement with the experimental peaks^[36] in the range of 200–350 nm confirming that the fullerene molecule absorbs mostly in the UV–Vis range of the electromagnetic spectrum. This makes us confident about the reliability of the model. The presence of the Be in the center of the molecule (Be@C60 in-1, Figure 2c) shows no remarkable changes in the spectrum of isolated C60 except for a slight red-shift of the E peak and for the presence of a further peak in the region between F and E, ascribable to the Be itself. The Be@C60 in-2 configuration (Figure 2d) follows the overall profile of Be@C60 in-1 with a broadening of all the peaks in the region between F and C. The Be in exohedral position with respect to the fullerene (Be@C60 out-1, Figure 2e) results in a different absorption profile from the endohedral ones, due to the splitting of the peaks between F and E and in the region between E and C together with a broadening in the region

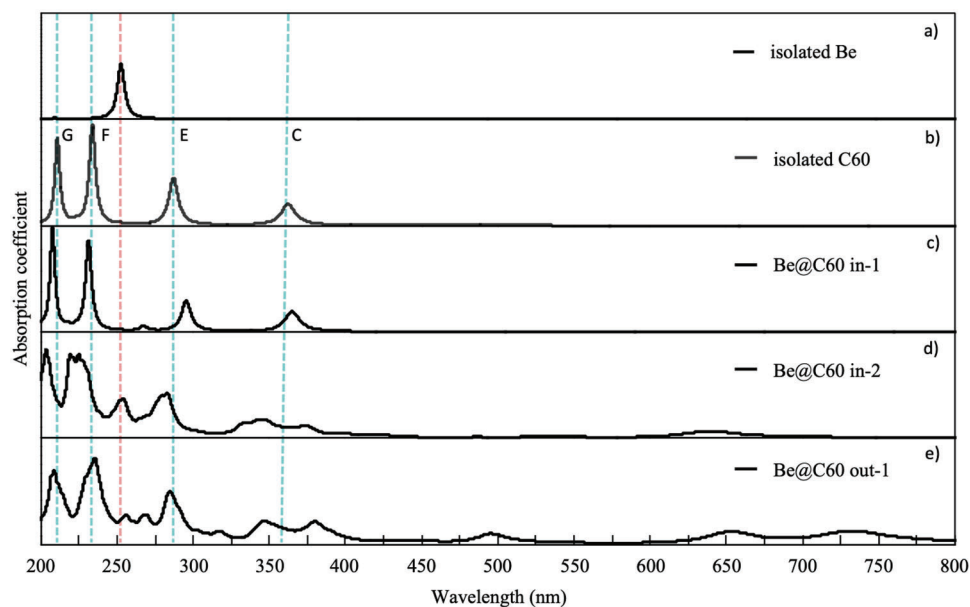


Figure 2. Absorption spectra for isolated Be (top panel, a), isolated C60 b), endohedral Be in-1 c) and in-2 d), and exohedral Be out-1 e), respectively. Vertical lines are a guide for the eye that discriminate among the main absorption peaks of both isolated C60 (cyan lines) and isolated Be (red line). Capital letters refer to the peaks in isolated fullerene (see text for explanation).

around C. The density of states (DOS) are helpful to discriminate the electronic transitions^[40] in order to interpret the spectra. The DOS and the projected DOS (PDOS) were computed for all the above-mentioned configurations and the results are summarized in **Figure 3**.

The endohedral Be@C60 in-1 shows, as expected, a profile where both C60 and Be hold essentially their pristine profile except for a slight Be-s—C-p hybridization in the HOMO region. Also, the HOMO and LUMO orbitals are shifted with respect to isolated C60. A more detailed analysis of the Lowdin charges and the PDOS reveals that a fraction (0.5e) of charge appears to be homogeneously distributed around the Be site in agreement with previous findings^[22] that suggest a slightly repulsive interaction between Be and the fullerene cage. Conversely, in the Be@C60 in-2 – where the Be atom is chemically bound to C – acceptor states with a s-Be—p-C nature appear in the C60 gap region. A charge transfer from s-Be to p-C is observed along with the splitting of s-Be and p-C around the HOMO. Also, the p-Be results

partially occupied around the Fermi energy. When Be is in the exohedral configuration (Be@C60 out-1), the HOMO-LUMO region has essentially a s-Be—p-C character with an involvement of p-Be orbitals, unlike the Be@C60 in-2 configuration.

Overall, the calculated absorption spectra indicate that, at least in principle, it is possible to detect the presence of undesired endohedral configurations from spectroscopic measurements.

4. Energy Barriers for Be Insertion

The analysis reported above confirms the occurrence of stable Be-C60 complexes, but it does not provide information on the energy barrier which must be overcome to form the complexes and on their expected lifetime. The kinetics of insertion/extraction is controlled by the corresponding energy barriers and their theoretical determination is the central parameter to tune the experimental ion implantation methodology. If the insertion energy is very high, then the implantation rate can be inefficient or induce

Table 2. Absorbance bands in nm. Present computed results for isolated C60, isolated Be, and Be@C60 complexes. In brackets, the average position of broadened peaks. Experimental measurements (exp.) and results obtained with similar methods (others) are reported for comparison.

	C	E	F	G
isolated Be			253	
isolated C60	362	287	234	211
Be@C60 in-1	365	295	267	209
Be@C60 in-2	<352>	282	256	225
Be@C60 out-1	<370>	286	<263>	209
Isolated Be exp. (2s2—2s2p) ^{a)}			235	
isolated C60 others ^{b)}	365	288	235	212
isolated C60 exp. ^{c)}	328	257	227	211

^{a)} References^[37,38]; ^{b)} Reference^[39]; ^{c)} Reference^[36].

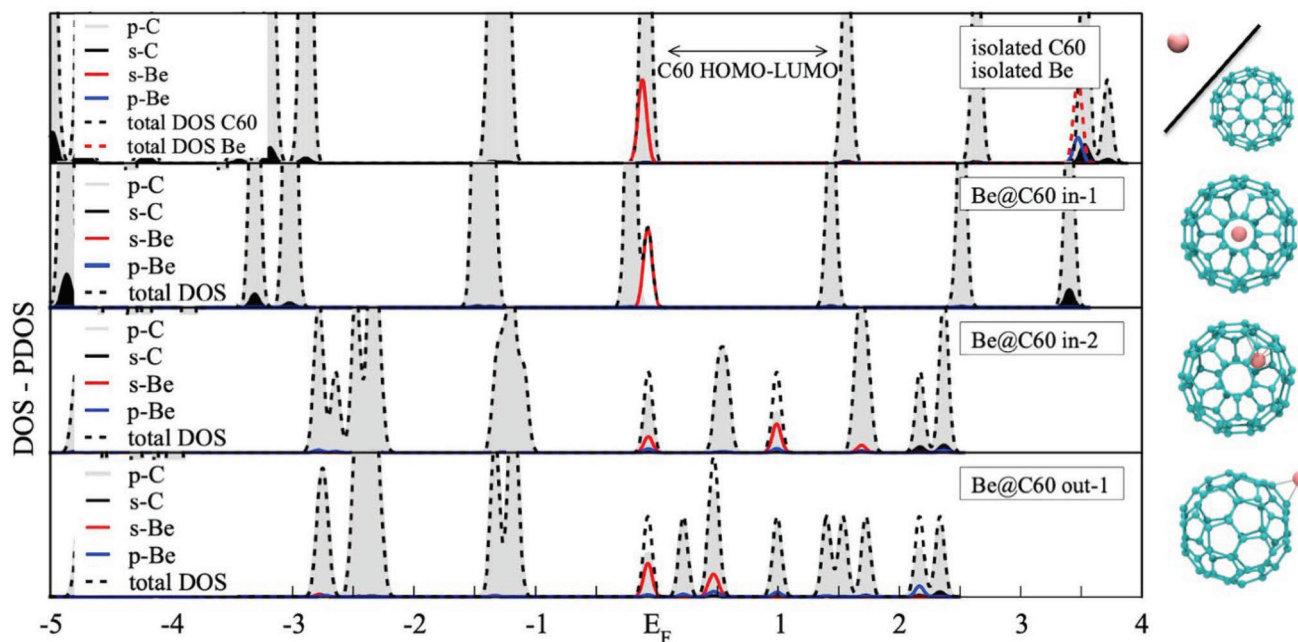


Figure 3. Top row: total and projected density of states (DOS/PDOS) for isolated C60 (2s in black and 2p in gray) and isolated Be (2s in red and 2p in blue). Other rows: DOS and PDOS of three different Be@C60 complexes as indicated; color code is the same as in the top row. Energies in eV are referred to the Fermi level E_F which is set to the highest occupied molecular state (HOMO).

damages to the fullerenes that may no longer be good containers for beryllium.

In order to calculate the optimal energy for Be insertion/extraction we have considered two kinds of paths in the configurational space: i) radial paths connecting the center of the fullerene to an external point at a distance 0.32 nm from the surface; ii) minimum energy paths between internal and external local minima obtained by the nudged elastic band method (NEB)^[41] as implemented in QE.^[34,35] For both types of paths, two cases were considered: i) passing through the center of a pentagonal ring; ii) passing through the center of a hexagonal ring. For the radial paths, the DFT energy is calculated at fixed atomic positions (unrelaxed). At variance, minimum energy paths obtained by the NEB method accounted for fully relaxed configurations: all atoms in the system were allowed to relax until the residual interatomic force became less than 10^{-4} eV \AA^{-1} . The NEB paths for the case of Be passing through the center of a hexagonal ring are reported in Figure 4 and described in the following, while the full set of curves is reported in Figure S1 (Supporting Information). We anticipate here that a model potential has been derived from ab initio data (details are provided in Supporting Information), and the energy barrier for implantation as calculated from model potential molecular dynamics (MD) simulations is also reported in Figure 4.

The NEB method allowed the estimate of the activation energy barrier for the transition from the initial state (exohedral configuration) to the final one (endohedral configuration) along the minimum energy path of the potential energy surface. The ab initio paths indicate that: i) local minima are present in the center and in proximity of the C60 both in endo- and exohedral configurations. ii) the activation barriers at the transition state correspond to the hexagonal and the pentagonal crossing rings, respectively,

and suggest the hexagonal ring of C60 as the favorite path for the Be atom to enter the molecule. iii) the order of magnitude of the energy barrier is ≈ 2.3 eV. This is an important result for the calibration of the experimental set up and the implantation energy.

The results obtained so far show that once that the Be is deposited inside the fullerene, it remains trapped therein because of the high energy barrier (2.7 eV) which is two orders of magnitude higher than the thermal energy at temperatures of biological interest. Nevertheless, during the implantation process there is the possibility for Be to form a stable exohedral complex (structure denoted as out-1 in Figure 1), due to an energy gain of 0.22 eV (see Table 1) upon binding with C60, which can be detrimental for practical applications. Washing the samples with proper solvents could be useful to remove outer Be, but it is important to discern if most complexes are endohedral as desired.

5. Finite Temperature Molecular Dynamics of Be Capture and Escape from C60 in Vacuo

A model potential has been derived from ab initio data similarly to previous studies.^[42] The GAFF^[43] model is used to describe C60 intramolecular forces, while the mixed C-Be interactions are modeled through a pairwise Buckingham potential, which consists in the sum of two terms, i.e., an exponential repulsive term characterized by the length scale plus a power law attractive term with dependence typical of dispersive interactions $U(x) = A \cdot e^{-\frac{x}{\rho}} - \frac{C}{x^6}$. The fitting procedure and parameters are reported in Supporting Information. We have calculated the barriers for Be implantation through 6- and 5-membered rings of C60. In Figure 4 we compare the classical model (dashed-dotted

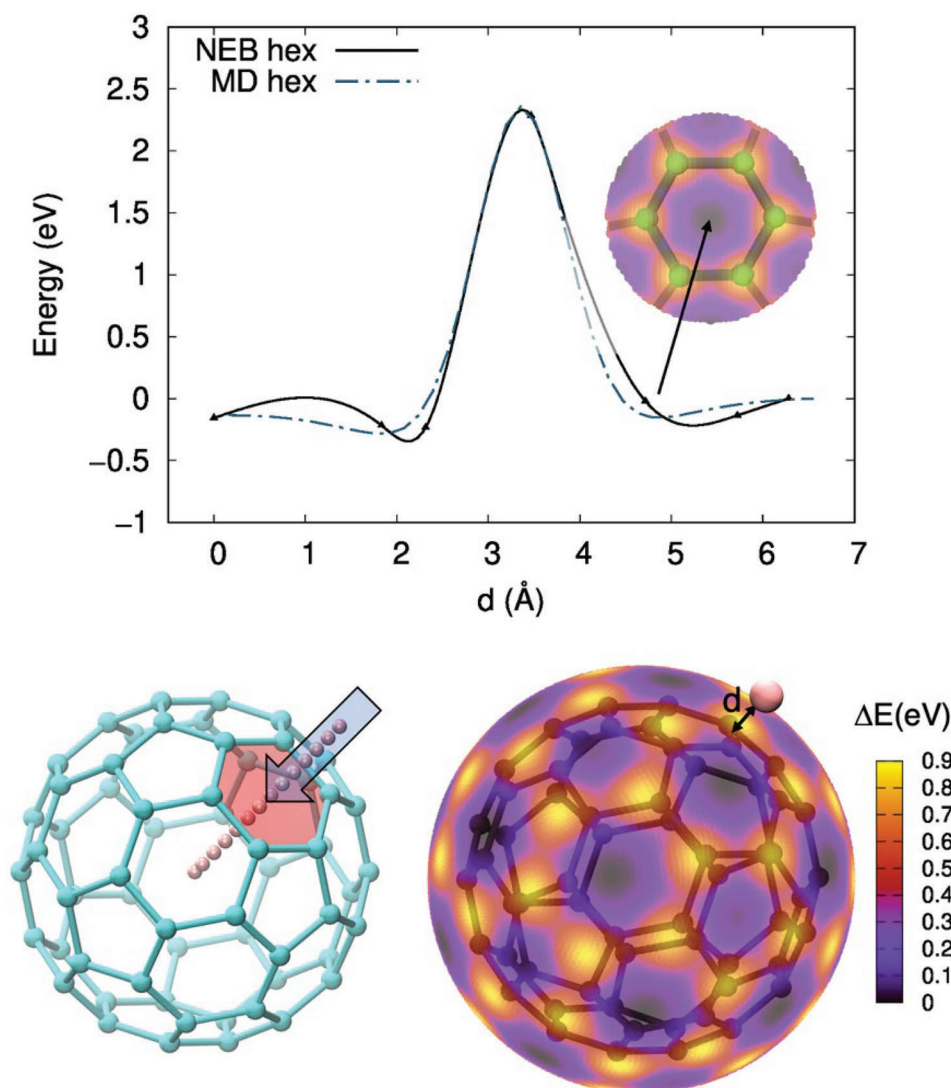


Figure 4. Top: minimum energy paths for hexagonal Be trajectory from ab initio NEB (black filled triangles; continuous line is a cubic spline interpolation) and from force-fields (dashed-dotted line). The C60 surface is at $d \sim 3.5$ Å. Bottom left: Be path from MD simulations; bottom right: energy map of Be-C60 interaction at different positions of the Be atom, at a distance $d \sim 0.8$ Å from the C60 surface. The inset of top panel shows the location of the minimum energy point in the center of a hexagon.

lines) with the ab initio NEB data (continuous lines) showing a good agreement for transition paths.

The developed classical force field was then used to study the Be implantation process into C60 molecules. As a first step, we calculated the Be-C60 interaction as a function of the position of the Be atoms on the fullerene surface. This was obtained by placing the Be atom on a regular spherical mesh at the distance of minimum energy (i.e., 0.79 Å) from the fullerene. The result is reported in Figure 4b, showing that energy minima are located at the center of hexagons and pentagons, as expected. To mimic the beam implantation process, Be atoms were placed at random positions within a circular region of variable radius r_B (ranging from 0.01 to 3.50 Å, i.e., the fullerene radius), with the center of the beam facing one of the C60 hexagons (being this the preferred location for entrance), and then accelerated at different kinetic

energies (ranging from 0.1 to 5.5 eV) toward the C60 molecule. A schematic of the simulation process is shown in Figure 5a. We define deflection as a trajectory during which Be does not enter inside the fullerene. The capture occurs when Be enters the C60 molecule and stays confined inside until the end of the run. Finally, exit is defined as a run in which, after entering C60, the Be atom is able to exit before the end of the run. Simulations were performed at zero and at room temperature; in the latter case we also distinguished the case of frozen rotations from the most general case in which the fullerene has freedom to rotate. Overall, more than $1.5 \cdot 10^6$ trajectories were calculated. The capture probability as a function of the beam radius r_B was computed at $T = 0$ K (results are reported in the Supporting Information). As the beam radius increases, the capture rate decreases since the probability for the Be atom to hit the C60 at the center of a

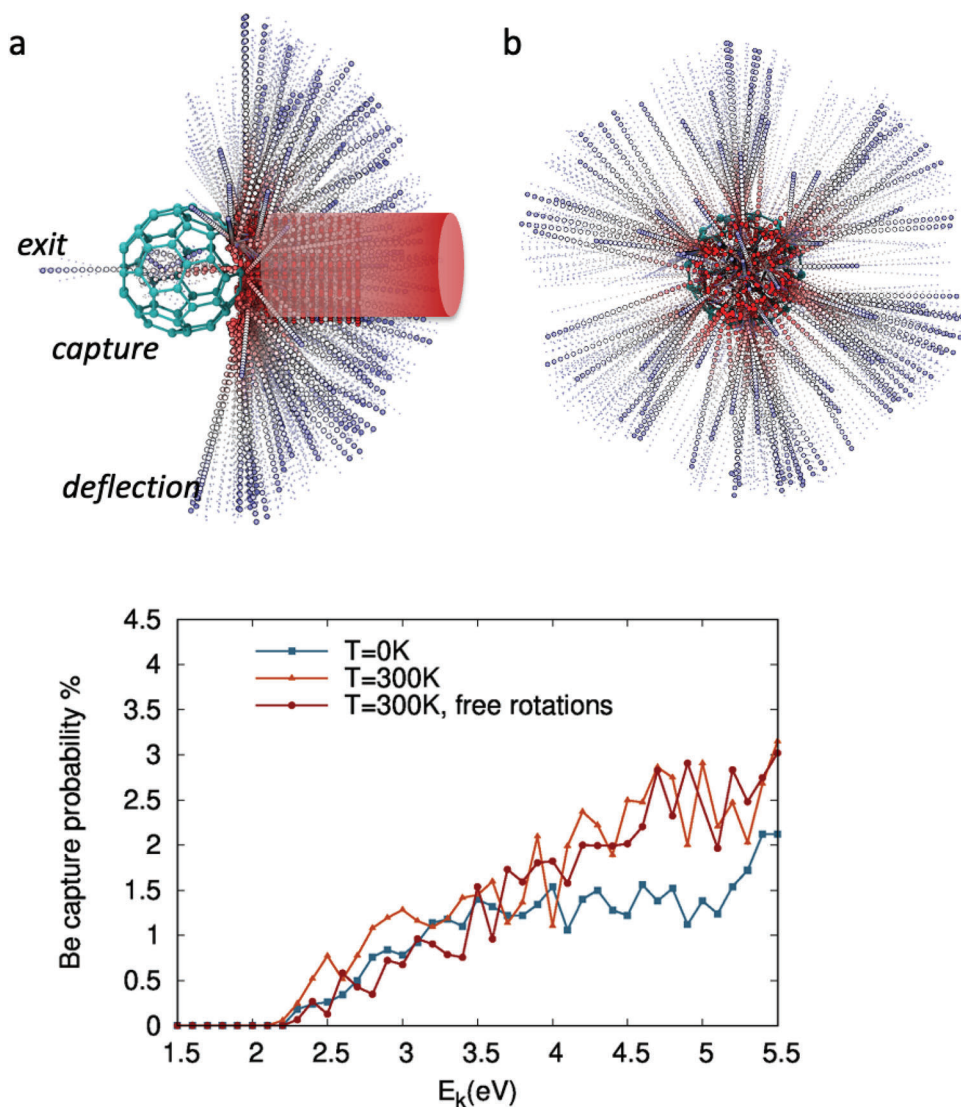


Figure 5. Top: schematic representation of the Be-deposition simulations a,b) (show side and top view, respectively) with three possible outcomes (deflection, capture and exit). Be atoms are represented in colors changing from red to blue according to the stage of the simulation (from the first to the last timesteps, respectively). The beam is shown as a red cylinder. Bottom: Be capture probability at different deposition energies E_k and different simulated conditions: $T = 0$ K (blue filled squares), $T = 300$ K with frozen rotations of C60 (orange filled triangles), $T = 300$ K with free rotations of C60 (red filled circles).

hexagon is lower. The case when the beam radius is r_B , i.e., equal to the fullerene size, corresponds qualitatively to the experimental case of a constant flux of incident Be atoms on a homogenous film of fullerenes. More realistic simulations are possible (considering a C60 film, the penetration depth, the Be-Be interactions, etc.) but beyond the scope of the present analysis.

Our MD results are reported in Figure 4c, showing that the temperature and rotations do not have a significant impact on the capture probability; as expected, the onset of Be capture corresponds to the calculated barrier of 2.3 eV. Our analysis indicates a relatively high capture probability ranging from 2 to 4% for energies between 4 and 6 eV and increasing at higher energies. However, implanting Be at much higher energies has the drawback of possibly damaging the fullerenes. In fact, C–C binding energy in C60 has been estimated by kinetic energy release distributions experiments to be ≈ 5 eV.^[44]

Once the Be ion is captured (forming the C60-Be endohedral complex) it is important to estimate the probability of escaping (i.e., the escape time is an estimate of lifetime of the Be-C60 complex). To this aim we performed a set of high temperature MD simulations and fitted the exit probability ν (i.e., the relative number of trajectories going out of the fullerene) by an Arrhenius law $\nu = \nu_0 e^{-\frac{E_B}{k_B T}}$, where k_B is the Boltzmann constant, T is the absolute temperature, ν_0 is the prefactor and E_B is the activation energy. The quantities ν_0 and E_B act as adjustable parameters of the fit. Be atom was placed inside the C60 at random positions and the complex was simulated at increasing temperature. For each temperature, 60 different starting configurations were considered. We explored a range of high temperatures which allow to observe exit events within the typical MD simulation time (nanoseconds). **Figure 6** shows a Be trajectory escaping from the

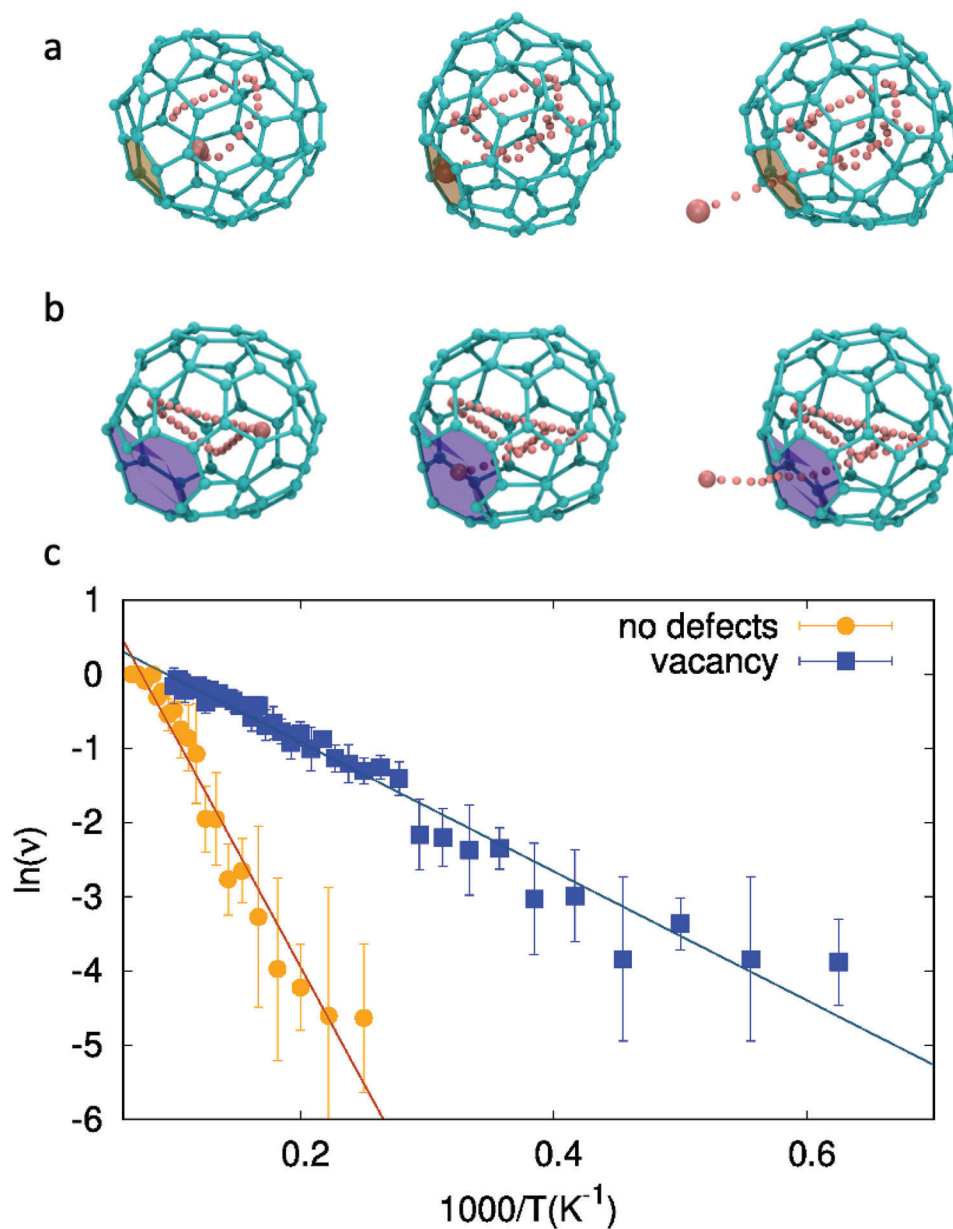


Figure 6. Snapshots of simulations of Be inside C60 a) and inside C59 b), and possible exit paths. c) Arrhenius plot of exit probability ν (number of exit events with respect to the total number of runs) versus inverse of temperature T (logarithmic scale is used for y axis). For both perfect and defected Be-fullerene complexes we performed a series of runs on a mesh of 40 temperatures \times 60 initial Be positions, for an overall simulation time of 50 ns.

C60 (a). From this analysis we obtained an activation energy for escape of $E_B = 2.7$ eV that agrees with the calculated NEB energy (notice that the in-2 configuration is ≈ 0.3 eV lower with respect to out-1 resulting in an escape barrier that is higher than the entrance one). By the fitted Arrhenius law, we extrapolate the lifetime of the Be@C60 at average human body temperature to be many orders of magnitude greater than human life expectancy, indicating that C60 is an ideal Be container for biomedical applications.

These results can be severely affected in case of defected fullerenes.^[45,46] We repeated the MD calculations by creating a carbon vacancy in the fullerene (i.e., C59). An example of escap-

ing trajectory is reported in Figure 6b. The energy barrier for exiting from the defected fullerene (C59) (see Figure 6c) is dramatically smaller, $E_B = 0.73$ eV and the estimated lifetime at room temperature goes down to only 30 s. These results highlight the importance of selecting high quality fullerene films to use as containers for Be atoms.

6. Be@C60 Complexes in Representative Biological Environments

The calculated high stability of endohedral ^7Be @C60 complex in vacuo makes it a good candidate for neutron capture therapy. By

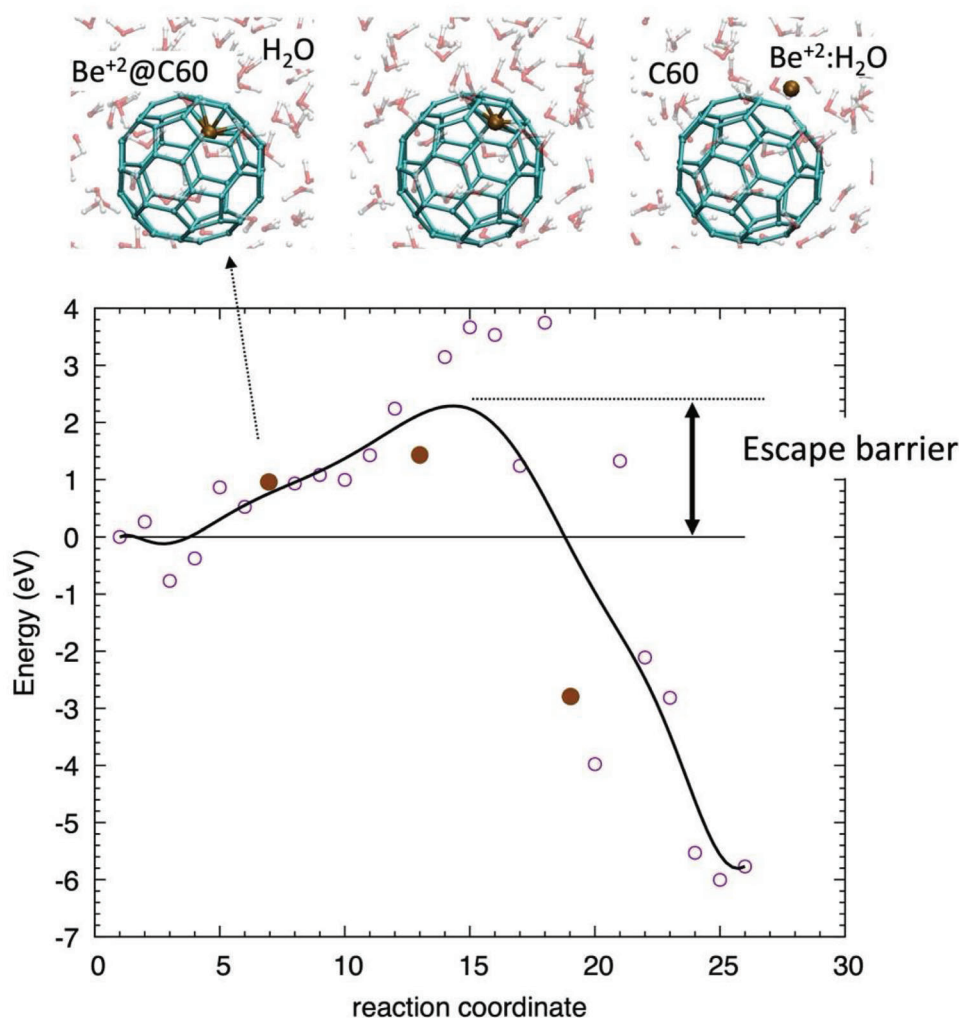


Figure 7. Top panels: snapshots of the exit trajectory of Be²⁺ from the fullerene (left) into water (right) obtained from a fictitious dynamics in which Be²⁺ is forced to exit by the application of suitable repulsive forces with C₆₀; Bottom panel: the corresponding energy profile of Be²⁺ as a function of the reaction coordinate shows the existence of a large energy barrier preventing the energetically favorable ion solvation; filled circles correspond to the energies of the top configurations.

suitable chemical functionalization of the fullerenes, it can be in principle possible to dissolve the Be@C₆₀ in the human body and to target the cancer cells. Under neutron flux the Be atoms decay emitting alpha particles and destroying the diseased cells. However, before any practical application, it is necessary to verify that such complexes are not toxic for the human body. In particular the Be@C₆₀ complex must be stable, not only in vacuo, but also in biological fluids (e.g., in the blood) without releasing the toxic beryllium atoms and without giving rise to undesired interactions with human tissues. A conclusive response on the health safety can only be obtained from in vivo experiments, but preliminary results can be already extracted from the present atomistic calculations. To this aim, we extend the force-field for Be-C in a similar fashion of previous studies^[47] to perform molecular dynamics simulations of Be²⁺@C₆₀ in water (see Supporting Material). We focus on charged 2+ beryllium that is the most relevant and dangerous and that, due to the large energy gain resulting from electrostatic interaction with water, is expected to have a strong driving force to escape from the fullerene.

Our findings show that also in water (H₂O) the Be atoms (no matter the charge state) are efficiently confined. This is confirmed by both molecular dynamics at high temperatures and by the calculation of the energy barrier for Be²⁺ to exit from C₆₀. The result is reported in bottom panel of **Figure 7** and is obtained by calculating the potential energy (circles) on a trajectory in which fictitious forces were applied to push Be out of the C₆₀. Snapshots of the Be²⁺@C₆₀:H₂O system during exit dynamics are reported in top panels of **Figure 7**. We find that also in water, the lowest energy path crosses the carbon hexagons.

The energy profile confirms a large energy barrier (>2 eV) to escape from C₆₀ and, correspondingly, a long lifetime of the Be²⁺@C₆₀ complex in water comparable to that of Be@C₆₀ in vacuo (many orders of magnitude longer than human life). The only qualitative difference of Be²⁺@C₆₀:H₂O with respect to the neutral case in vacuo (compare **Figures 7** and **4**) is that the energy in water steeply decreases out of the fullerene because of the efficient Be²⁺ solvation.

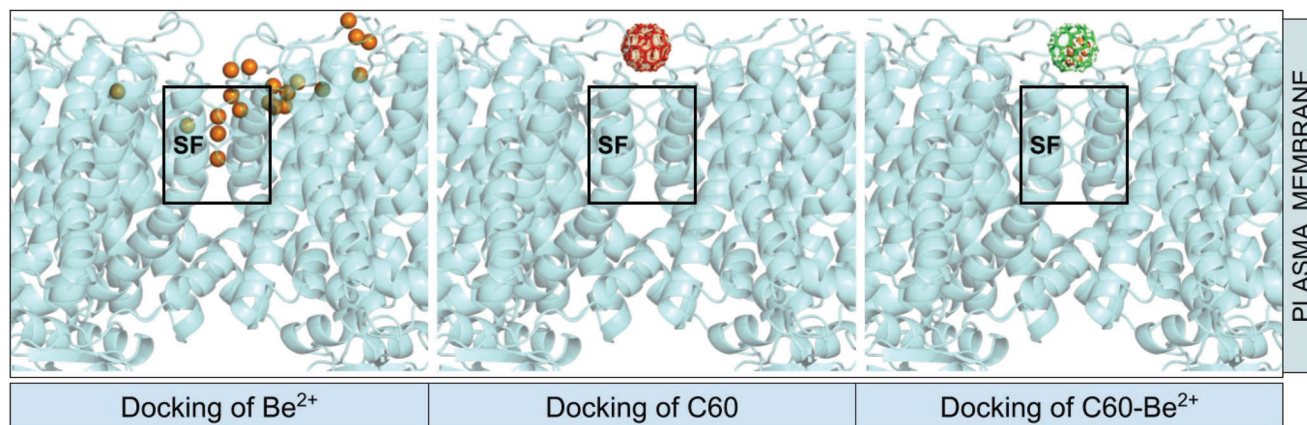


Figure 8. Optimal 20 poses from blind docking of Be^{2+} (left), C60 (middle), and C60-Be^{2+} (right). The selectivity filter of Slo1 is marked with a black box (SF).

In conclusion, the Be atoms remain safely confined inside the fullerene even in aqueous environments.

The calculated beryllium-oxygen distance during the dynamics is greater than 4 Å suggesting that C60 cage isolates the Be and prevents the formation of undesired bonds with the atoms of the surrounding chemical environment. In order to further investigate the possible effects on biological matter we study the interaction of the endohedral complex $\text{Be}^{2+}@\text{C60}$ with a representative protein. A very convenient and computationally inexpensive way of checking some fundamental molecule-protein interactions comes in the form of molecular docking. In molecular docking, the optimal target structure (in this case the protein) is scanned for locations of minimal docking score for a particular ligand. For this occasion, we have selected a Ca^{2+} -dependent K⁺-channel, Slo1 (PDB ID: 5TJ6).^[48] Slo1 is chosen because it is controlled by calcium ions, and one of the toxicity aspects of Be^{2+} is the replacement of the Ca^{2+} in various physiological processes.^[49] Furthermore, docking sites on the Slo1 were well examined in the literature,^[50] so we could use it as a docking target with great confidence.

First, we have docked only Be^{2+} with the most prominent positions shown on the left of **Figure 8**. We see that the Be^{2+} can penetrate the selectivity filter of the Slo1. Some of the poses show docking laterally on the protein's extracellular surface. On the other hand, C60 (middle panel) stays outside of the cell as its size doesn't allow passage through the selectivity filter. All the poses are found in the same location on the top of the selectivity filter, probably due to the high symmetry. Finally, on the right, we see that the $\text{Be}^{2+}@\text{C60}$ complex behaves in a practically identical way as the empty C60, thus showing that the fullerene can efficiently screen the Be^{2+} thus preventing possible toxic effects.

7. Conclusions

Present study shows that stable $\text{Be}@\text{C60}$ endohedral complexes can be obtained by implanting Be atoms at energies >2.3 eV. This could be practically realized for example with current laser-based implantation technologies. Furthermore, by calculating optical absorption by TDDFT, we show that it is possible to distinguish endohedral complexes from exohedral ones by non-destructive optical spectroscopy. Overall, we conclude that it is possible to

encapsulate Be atoms into fullerenes, which prove to be efficient molecular containers with practically zero probability of release of the toxic beryllium radionuclides at typical conditions of biological systems. The confining efficiency decreases dramatically for defected fullerenes that accordingly must be carefully avoided (either during synthesis or by post-processing) together with metastable complexes in which Be can be easily released. Preliminary simulations of $\text{Be}@\text{C60}$ complexes in aqueous solutions and plasma membranes confirm that the C60 efficiently confines Be (either neutral or charged) also in biological environments and it likely prevents Be toxicity.

In conclusion, we provided a solid theoretical assessment of the possibility of using fullerenes as containers for Be atoms for applications to neutron capture therapies.

Supporting Information. Additional properties of stationary geometries, derivation and parameters of the model potential for Be-fullerene interaction and Be capture probability for different beam radii r_B at zero temperature can be found in the Supporting Information PDF file.

Supporting Information

Supporting Information is available from the Wiley Online Library or from the author.

Acknowledgements

The authors acknowledge CNR for funding within "Accordo bilaterale CNR-RFBR" through Project B55F21000620005 "Development of laser implantation technology of production of fullerene containers for prospective Be neutron capture therapy of cancer" and CINECA for computational support through ISCRA initiatives (FFBeNCT, SIPS-MD, BeNCT-FF, BeNCT-S). AM acknowledges financial support from ICSC – Centro Nazionale di Ricerca in High Performance Computing, Big Data and Quantum Computing, funded by European Union – NextGenerationEU – PNRR, Missione 4 Componente 2 Investimento 1.4 (Project B93C22000620006).

Conflict of Interest

The authors declare no conflict of interest.

Author Contributions

I.B. and A.S. contributed equally to this work. I.B., M.C., A.S., and A.M. conceived the work. I.B. and A.S. performed electronic structure calculations. S.M. performed MD and docking analysis of Be complexes on proteins. C.C. performed MD simulations of implantation and exit probability in vacuo. G.C. performed MD simulations of complexes in water. A.M. developed the force fields, performed MD calculations of energy profiles in vacuo and water and coordinated the project. C.C. collected all the results and redacted the first version of the manuscript. The final manuscript was written through contributions of all authors. All authors have given approval to the final version of the manuscript.

Data Availability Statement

The data that support the findings of this study are available from the corresponding author upon reasonable request.

Keywords

Density Functional Theory, molecular dynamics, multiscale modeling, Neutron Radiation Therapy

Received: April 5, 2023

Revised: May 16, 2023

Published online:

- [1] W. Cai, C. H. Chen, N. Chen, L. Echegoyen, *Acc. Chem. Res.* **2019**, *52*, 1824.
- [2] J. R. Heath, S. C. O'Brien, Q. Z. Y. Liu, R. F. Curl, F. K. Tittel, R. E. Smalley, H. W. Kroto, *J. Am. Chem. Soc.* **1985**, *107*, 7779.
- [3] Y. Chai, T. Guo, C. Jin, R. E. Haufler, L. P. F. Chibante, J. Fure, L. Wang, J. M. Alford, R. E. Smalley, *J. Phys. Chem.* **1991**, *95*, 7564.
- [4] M. Saunders, H. A. Jiménez-Vázquez, R. J. Cross, S. Mroczkowski, M. Gross, D. E. Giblin, R. J. Poreda, *J. Am. Chem. Soc.* **1994**, *116*, 2193.
- [5] T. Ohtsuki, K. Masumoto, K. Ohno, Y. Maruyama, Y. Kawazoe, K. Sueki, K. Kikuchi, *Phys. Rev. Lett.* **1996**, *77*, 3522.
- [6] S. C. Benjamin, A. Ardavan, G. A. D. Briggs, D. A. Britz, D. Gunlycke, J. Jefferson, M. A. G. Jones, D. F. Leigh, B. W. Lovett, A. N. Khlobystov, S. A. Lyon, J. J. L. Morton, K. Porfyrakis, M. R. Sambrook, A. M. Tyrshkin, *J. Phys.: Condens. Matter* **2006**, *18*, S867.
- [7] S. Zhou, J. Yuan, Z. Y. Wang, K. Ling, P. X. Fu, Y. H. Fang, Y. X. Wang, Z. Liu, K. Porfyrakis, G. A. D. Briggs, S. Gao, S. D. a Jiang, *Angew. Chem., Int. Ed.* **2022**, *61*, 202115263.
- [8] R. Cui, J. Li, H. Huang, M. Zhang, X. Guo, Y. Chang, M. Li, J. Dong, B. Sun, G. Xing, *Nano Res.* **2014**, *8*, 1259.
- [9] T. Li, H. C. Dorn, *Small* **2017**, *13*.
- [10] A. M. Scorciapino, C. Nunes, M. Ceccarelli, E. Tkalya, I. Bodrenko, *J. Nanosci. Nanotechnol.* **2021**, *21*, 2939.
- [11] V. I. Kukulin, A. V. Bibikov, E. V. Tkalya, M. Ceccarelli, I. V. Bodrenko, "7Be and 22Na radionuclides for a new therapy of cancer." arXiv preprint arXiv:1907.05934 and accepted for publication in *Biomolecular Concepts* **2023**.
- [12] G. L. Locher, *Am. J. Roentgenol.* **1936**, *36*, 1.
- [13] L. E. Farr, W. H. Sweet, H. B. Locksley, J. S. Robertson, *Trans. Am. Neurol. Assoc.* **1954**, *13*, 110.
- [14] D. Nathan Slatkin, M. J. Javid, D. D. Joel, J. Abraham Kalef-Ezra, R. Ma, L. E. Feinendegen, J. A. Laissue, *J. Neurol. Neurobiol.* **2017**, *3*, 1.
- [15] R. F. Barth, P. Mi, W. Yang, *Cancer Commun.* **2018**, *38*, 1.
- [16] R. F. Barth, J. A. Coderre, M. G. H. Vicente, T. E. Blue, *Clin. Cancer Res.* **2005**, *11*, 3987.
- [17] R. F. Barth, M. G. H. Vicente, O. K. Harling, W. S. Kiger, K. J. Riley, P. J. Binns, F. M. Wagner, M. Suzuki, T. Aihara, I. Kato, S. Kawabata, *Radiat. Oncol.* **2012**, *7*, 146.
- [18] R. L. Moss, *Appl. Radiat. Isot.* **2014**, *88*, 2.
- [19] I. Tomandl, J. Vacik, U. Köster, L. Viererbl, E. A. Maugeri, S. Heintz, D. Schumann, M. Ayrarov, J. Ballof, R. Catherall, K. Chrysalidis, T. Day Goodacre, D. Fedorov, V. Fedosseev, K. Johnston, B. Marsh, S. Rothe, J. Schell, C. Seiffert, *Phys. Rev. C* **2019**, *99*, 014612.
- [20] P. E. Koehler, C. D. Bowman, F. J. Steinkruger, D. C. Moody, G. M. Hale, J. W. Starner, S. A. Wender, R. C. Haight, P. W. Lisowski, W. L. Talbert, *Phys. Rev. C* **1988**, *37*, 917.
- [21] T. D. Luckey, B. Venugopal, *Physiologic and Chemical Basis for Metal Toxicity*, Springer, New York **1977**.
- [22] J. Lu, Y. Zhou, X. Zhang, X. Zhao, *Chem. Phys. Lett.* **2002**, *352*, 8.
- [23] E. V. Tkalya, A. V. Bibikov, I. V. Bodrenko, *Phys. Rev. C Nucl. Phys.* **2010**, *81*, 024610.
- [24] E. V. Tkalya, A. V. Avdeenkov, A. V. Bibikov, I. V. Bodrenko, A. V. Nikolaev, *Phys. Rev. C Nucl. Phys.* **2012**, *86*, 014608.
- [25] C. A. Simion, A. Berinde, *J. Radioanal. Nucl. Chem.* **2006**, *270*, 621.
- [26] J. Yin, S. Zhang, Z. Sun, X. Li, *J. Mol. Struct.* **2007**, *816*, 53.
- [27] M. J. Frisch, G. W. Trucks, H. B. Schlegel, G. E. Scuseria, M. A. Robb, J. R. Cheeseman, G. Scalmani, V. Barone, G. A. Petersson, H. Nakatsuji, X. Li, M. Caricato, A. V. Marenich, J. Bloino, B. G. Janesko, R. Gomperts, B. Mennucci, H. P. Hratchian, J. V. Ortiz, A. F. Izmaylov, J. L. Sonnenberg, D. Williams-Young, F. Ding, F. Lipparini, F. Egidi, J. Goings, B. Peng, A. Petrone, T. Henderson, D. Ranasinghe, et al., GaussianTM 16 Revision C.01 **2016**.
- [28] J. P. Perdew, K. Burke, M. Ernzerhof, *Phys. Rev. Lett.* **1996**, *77*, 3865.
- [29] S. Grimme, S. Ehrlich, L. Goerigk, *J. Comput. Chem.* **2011**, *32*, 1456.
- [30] A. D. Becke, *J. Chem. Phys.* **1993**, *98*, 6264.
- [31] P. C. Hariharan, J. A. Pople, *Theor. Chim. Acta* **1973**, *28*, 213.
- [32] T. Morisato, K. Ohno, T. Ohtsuki, K. Hirose, M. Sluiter, Y. Kawazoe, *Phys. Rev. B Condens. Matter Mater. Phys.* **2008**, *78*, 125416.
- [33] C. Caddeo, G. Mallocci, F. De Angelis, L. Colombo, A. Mattoni, *Phys. Chem. Chem. Phys.* **2012**, *14*, 14293.
- [34] P. Giannozzi, S. Baroni, N. Bonini, M. Calandra, R. Car, C. Cavazzoni, D. Ceresoli, G. L. Chiarotti, M. Cococcioni, I. Dabo, A. Dal Corso, S. De Gironcoli, S. Fabris, G. Fratesi, R. Gebauer, U. Gerstmann, C. Gougoussis, A. Kokalj, M. Lazzeri, L. Martin-Samos, N. Marzari, F. Mauri, R. Mazzarello, S. Paolini, A. Pasquarello, L. Paulatto, C. Sbraccia, S. Scandolo, G. Sclauzero, A. P. Seitsonen, et al., *J. Phys. Condens. Matter* **2009**, *21*, 395502.
- [35] P. Giannozzi, O. Andreussi, T. Brumme, O. Bunau, M. Buongiorno Nardelli, M. Calandra, R. Car, C. Cavazzoni, D. Ceresoli, M. Cococcioni, N. Colonna, I. Carnimeo, A. Dal Corso, S. De Gironcoli, P. Delugas, R. A. Distasio, A. Ferretti, A. Floris, G. Fratesi, G. Fugallo, R. Gebauer, U. Gerstmann, F. Giustino, T. Gorni, J. Jia, M. Kawamura, H. Y. Ko, A. Kokalj, E. Küçükbenli, M. Lazzeri, et al., *J. Phys. Condens. Matter* **2017**, *29*, 465901.
- [36] S. Leach, M. Vervloet, A. Desprès, E. Bréheret, J. P. Hare, T. J. Dennis, H. W. Kroto, R. Taylor, D. R. M. Walton, *Chem. Phys.* **1992**, *160*, 451.
- [37] R. E. Irving, M. Henderson, L. J. Curtis, I. Martinson, P. Bengtsson, *Can. J. Phys.* **2011**, *77*, 137.
- [38] G. Tachiev, C. F. Fischer, *J. Phys. B: At., Mol. Opt. Phys.* **1999**, *32*, 5805.
- [39] J. Ren, S. Meng, E. Kaxiras, *Nano Res.* **2012**, *5*, 248.
- [40] L. Giacopetti, A. Nevin, D. Comelli, G. Valentini, M. B. Nardelli, A. Satta, *AIP Adv.* **2018**, *8*, 065202.
- [41] G. Henkelman, H. Jónsson, *J. Phys. Chem.* **2000**, *113*, 9978.
- [42] T. Hata, G. Giorgi, K. Yamashita, C. Caddeo, A. Mattoni, *J. Phys. Chem. C* **2017**, *121*, 3724.
- [43] J. Wang, R. M. Wolf, J. W. Caldwell, P. A. Kollman, D. A. Case, *J. Comput. Chem.* **2004**, *25*, 1157.
- [44] C. Lifshitz, *Int. J. Mass Spectrom.* **2000**, *198*, 1.
- [45] Y. H. Hu, E. Ruckenstein, *J. Chem. Phys.* **2004**, *120*, 2759.

- [46] Y. H. Hu, E. Ruckenstein, *J. Chem. Phys.* **2003**, *119*, 10073.
- [47] C. Caddeo, D. Marongiu, S. Meloni, A. Filippetti, F. Quochi, M. Saba, A. Mattoni, *Adv. Mater. Interfaces* **2019**, *6*, 1801173.
- [48] X. Tao, R. K. Hite, R. MacKinnon, *Nature* **2017**, *541*, 46.
- [49] J. Elguero, I. Alkorta, *Struct. Chem.* **2023**, *34*, 391.
- [50] M. Bachmann, A. Rossa, T. Varanita, B. Fioretti, L. Biasutto, S. Milenkovic, V. Checchetto, R. Peruzzo, S. A. Ahmad, S. H. Patel, R. Lukowski, M. J. Edwards, M. Ceccarelli, E. Gulbins, M. Zoratti, A. Mattarei, I. Szabo, *Cell Death Dis.* **2022**, *13*, 1055.